Nanoscale

Accepted Manuscript

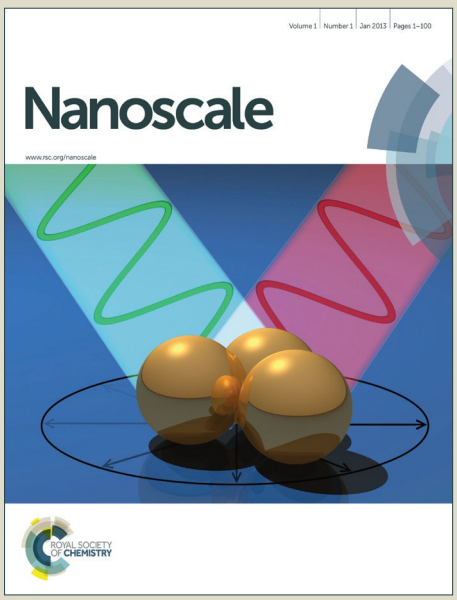

ROYAL SOCIETY OF CHEMISTRY

www.rsc.org/nanoscale

Nanoscale

RSCPublishing

PAPER

3D Intra-Stacked CoO/Carbon Nanocomposites Welded by Ag Nanoparticles for High-Capacity, Reversible Lithium Storage

Cite this: DOI: 10.1039/x0xx00000x

Received ooth January 2012,
Accepted ooth January 2012

DOI: 10.1039/x0xx00000x

www.rsc.org/

Changju Chae[a], Ki Woong Kim[a], Sue Jin Kim[a], Daehee Lee[b], Yejin Jo[a], Young Jun Yun[a], Jooho Moon[b], Youngmin Choi,[a] Sun Sook Lee[a,]*, Sungho Choi[a,]*, Sunho Jeong[a,]*

A wet-chemical, facile strategy is proposed for forming three-dimensionally intra-structured nanocomposites to facilitating development of high performance anodes for lithium ion batteries. The nanocomposites are composed of cobalt oxide nanoparticles, reduced graphene oxides, and Ag nanoparticles, and all the constituent materials are incorporated homogenously in a layer-by-layer structured geometry by a simple sono-chemical hybridizing process in a single, one-pot batch. Herein, it is revealed that the homogenously intra-stacked oxide, carbon, and metallic phases play critical roles in determining electrochemical performance (i.e., high capacity, rate capability, and cycling stability) of nanocomposite-based anodes, owing to the characteristic chemical/physical nature of constituent materials welded by partial melting of the metallic nanoparticles. In particular, by virtue of a characteristic role of nano-Ag phase in suppressing the irreversible capacity, a critical drawback for metal oxide-based anodes, excellent capacities are demonstrated (983 and 770 mAh/g at current densities of 100 and 2000 mA/g, respectively).

Introduction

Lithium ion batteries (LIBs) are currently the preferred power source not only for general consumer electronics, but also for upcoming electric vehicles. To date, a number of materials and their composites have been exploited as anodes for LIBs. These have included graphitic carbons, Si, Sn, and transition metal oxides (SnO_2, CoO, Co_3O_4, NiO, TiO_2, Fe_2O_3, MnO_2), and their selection has been based upon the study of the electrochemical mechanisms of intercalation, alloying, or conversion reaction.[1] Among them, metal oxides have attracted tremendous attention as candidate materials for high-density energy-storage systems. This interest is due to their high theoretical capacity much higher than that (372 mAh/g) of graphite.[2] However, for transition metal oxide-based anodes, the charge/discharge electrochemical reactions are accompanied by repeated volume-expansion and contraction. This inevitably leads to electrode-pulverization and morphological degradation of inter-particular networked structures, resulting in significantly low cycling stability along with irreversible capacity loss, a critical intrinsic impediment to wider use of metal oxide-based anodes.

Recently, the use of carbon-incorporated nanocomposites, through in-situ spatial distribution of metal oxides on graphene and/or graphene oxides, has been suggested as one strategy for stabilizing the structural deformation.[3-7] For in situ synthetic schemes, heterogeneous nucleation is triggered on the surface of carbon materials. There, its lower activation energy (compared with homogenous nucleation in free spaces) facilitates the formation of planar-structured oxide-carbon composites with high capacity and acceptable cycling stability. However, in such 2D-based composites, the electrical conduction pathways in an overall electrode would not be established due to the lack of electrically networked structures between neighboring oxide-incorporated carbon sheets. In contrast, lithium-ion conduction can be tailored with sophisticated nano-structural design of nanostructures. This structural limitation results in the significant degradation of capacity at high current densities. Alternative, interconnected oxide-carbon composite mixtures have been exploited that involve newly developed chemical pathways including co-synthesis of oxides and carbons,[8,9] formation of intact aggregates of graphene encapsulated oxide nanoparticles,[10] implementation of oxides in carbon nanohorns,[11] surfactant-assisted in situ synthesis,[12] and electrostatic hybridization.[13,14] The paramount importance of forming the structure-engineered homogenous nanocomposites has been proven by the fact that the further improved electrochemical performance with a high rate capability even over 2,000 mAg^{-1} could be manipulated in electrodes based on complete core-shell structured metal oxide-carbon composites[15-17] or chemically incorporated metal oxides in pre-structured ordered mesoporous carbon nanorods[18,19].

Herein, we report a facile method for forming 3D hierarchical networked CoO-carbon nanocomposites using

metal nanoparticles as nano-welders. In contrast to previous complicated approaches, it is demonstrated that a water soluble graphene oxide (GO) is capable of being mixed with non-polar olate-capped Ag nanoparticles even by a scalable, simple sonication-based mixing procedure involving with the addition of a proper co-solvent. The metal nanoparticles undergo vigorous diffusion behavior at temperatures below 300 ^{o}C, allowing thermally activated interfacial welding of neighboring CoO nanoparticles and at hetero-junction surfaces of CoO nanoparticles and GOs. In addition to the morphological contribution of nano-phase Ag, it is revealed that welded Ag-phase plays a predominant role in resolving the critical issue of high irreversible capacity loss. This simple approach based on multifunctional hybridization of materials with characteristic individual roles, enables the formation of LIB-anode materials with capacities of 983 and 770 mAh/g, at current densities of 100 and 2000 mA/g, respectively.

Experimental

Synthesis of CoO nanoparticles

Co(III) acetylacetonate ($Co(C_5H_7O_2)_3$, 98%), octylamine ($C_8H_{17}NH_2$, 99%), oleic acid ($C_{18}H_{34}O_2$, 90%), phenylhydrazine ($C_6H_5NHNH_2$, 97%), and toluene ($C_6H_5CH_3$, anhydrous, 99.8%) were purchased from Aldrich. All chemicals were used as received without further purification. The 20.4 g of Co acetylacetonate and 27.6 g of oleic acid were poured into a four-neck round-bottomed flask containing 73.6 g of octylamine. The flask was fitted with a reflux condenser and a mechanical stirrer. The solution was heated at 90 ^{o}C and purged with flowing Ar for 1 h. Then, 87.4 g of phenylhydrazine was injected at a temperature of 150 ^{o}C, with an injection rate of 0.5 ml/min. After completing the synthetic reaction, the synthesized CoO nanoparticles were separated by centrifugation and washed with toluene in air. The CoO nanoparticles were stored in toluene under air.

Synthesis of Ag nanoparticles

Ag nitrate ($AgNO_3$, 99.9%, Kojima Chemicals Co., LTD.), octylamine ($C_8H_{17}NH_2$, 99%, Aldrich), oleic acid ($C_{18}H_{34}O_2$, 90%, Aldrich), phenylhydrazine ($C_6H_5NHNH_2$, 97%, Aldrich) and toluene ($C_6H_5CH_3$, anhydrous, 99.8%, Aldrich) were used as received without further purification. Ag nanoparticles were synthesized, via chemical reduction of Ag ions, in octylamine under ambient atmosphere. 9.5 g of silver nitrate and 25.1 g of oleic acid were added to a 3-necked round-bottom flask containing 73.6 g of octylamine. The solution was stirred with a magnetic bar, and the flask was fitted with a reflux condenser. The solution was maintained at 60 ^{o}C for 20 min and heated to 80 ^{o}C. Next, 87.4 g of phenylhydrazine was injected at a rate of 5 ml/min. Then, the reaction continued for 60 min. After completion of the synthetic reaction, the synthesized Ag nanoparticles were separated by centrifugation and washed with a mixture of toluene and ethanol in air. The Ag nanoparticles were stored in toluene under air.

Synthesis of graphene oxides

Graphene oxides (GOs) were prepared from natural graphite flakes (Sigma Aldrich) by subsequent reaction of oxidation/exfoliation, using a modified Hummers method. A mixture of natural graphite flakes (5.0 g) and $NaNO_3$ (3.75 g) was inserted in a 2 L round-bottom flask containing 375 ml of H_2SO_4 (95%) and stirred in an ice bath. 22.5 g of $KMnO_4$ was added slowly, while the reaction temperature was kept below 20 °C. Then, the flask was placed in an oil bath at 30 ^{o}C for two days. After the flask was cooled in air, 700 ml of 5 wt% H_2SO_4 was slowly added to the flask, and then stirred for 2 h. Next, 15 ml of 30 wt% H_2O_2 was slowly added while the color of the suspension changed from dark brown to yellow, and stirring continued for 2 h. The as-obtained graphite oxide was purified by centrifugation several times in distilled water. GO sheets were exfoliated by ultra-sonication. The products were re-dispersed in distilled water.

Preparation of 3D nanocomposites (3D-NCs)

Ag nanoparticles were collected by centrifugation at 24,000 rpm for 15 min, using a mixture of toluene and ethanol (1:1 v/v). For obtaining homogeneity in the mix of different materials, wet precipitates not subjected to a drying process, were used for further experiments. The wet precipitates, obtained after completely removing the supernatant solutions, still contained some solvent; thus, the fraction of solvents was measured by weighing as-precipitated and fully dried powders for five different samples. The solvent fraction in Ag nanoparticle precipitate was 13.5 wt%, and the yield after thermal treatment at 300 ^{o}C was 89.5 wt%. Then, 40 ml of aqueous GO solution (3 mg/ml) was centrifuged at 24,000 rpm for 30 min after adding 80 ml of methanol. The resulting GO precipitates were re-dispersed in 120 ml of methanol and centrifuged again at 24,000 rpm for 30 min, to remove the water inside the GO precipitates. The solvent fraction in GO precipitate was 95.9 wt% and the yield after thermal treatment at 300 ^{o}C was 38.9 wt%. The CoO nanoparticles were collected by centrifugation at 24,000 rpm for 15 min. The fraction of toluene was 15.3 wt% and the yield after thermal treatment at 300 ^{o}C was 94.4 wt%. The Ag wet precipitates were dispersed in dichlorobezene (DCB) by sonication, and then the wet GO precipitates were added in the prepared Ag solution with the addition of N-methyl-2-pyrrolidone (NMP, 99.5%, Aldrich). The CoO wet precipitates were dispersed in DCB by sonication. The CoO suspension and Ag/GO mixture were homogenized to form a homogeneous solution by sonication. The resulting composite materials were collected by centrifugation at 24,000 rpm for 20 min, followed by a vacuum drying at 80 ^{o}C for 72 h, and a thermal annealing at 300 ^{o}C for 1 h under flowing Ar gas (at a rate of 100 sccm).

Fabrication of anodes for lithium-ion batteries

Electrochemical tests were conducted using CR2032 coin cells with Li metal as a reference electrode. The working electrodes were prepared by casting pastes onto a copper-foil current collector. The pastes were composed of active materials (CoO nanoparticle, Ag nanoparticle, Ag-free CoO/RGO composite, and 3D-NCs), Super-P carbon black, polyvinylidene fluoride (PVDF, Kureha KF-1100) as a binder, and NMP as a solvent at a ratio of 80 (active material): 10 (Super-P): 10 (PVDF) in weight. For the preparation of 3D-NC/MWCNT pastes, 0.15 g of 3D-NCs and 0.01 g of MWCNT (CM 150, Hanhwa Nanotechnology) were dispersed in NMP using sonication; then the suspension was centrifuged at 24,000 rpm for 30 min and dried in vacuum oven at 80 ^{o}C for 12 h. The composition in a paste was 75 (3D-NC): 5 (MWCNT): 10 (Super-P): 10 (PVDF)

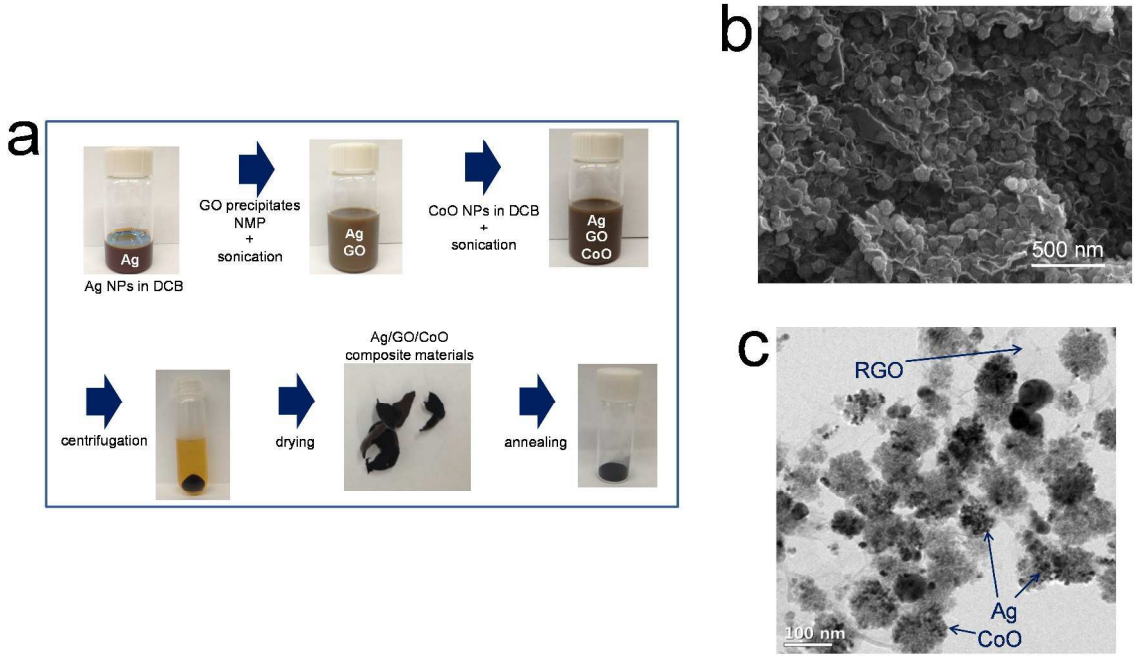

Figure 1. (a) Photographs showing the sequential procedures for preparing 3D-NCs. (b) SEM and (c) HRTEM images for 3D-NCs prepared by mixing Ag nanoparticles, graphene oxides, and CoO nanoparticles.

in weight. All the working electrodes were pressed and vacuum dried at 120 °C for 12 h. A Celgard 2400 was used as separator, and 1 M $LiPF_6$ in a mixture of ethylene carbonate/diethyl carbonate (EC/DEC, 1:1 v/v) was used as electrolyte. The cells were assembled in an Ar-filled glove box. The galvanostatic charge-discharge profile, cycling performance, and rate performance were investigated in the voltage range of 0.01–3.0 V vs. Li^+/Li at a current density of 0.1–2 A/g, using a battery-testing equipment (TOSCAT-3100, Toyo Co. Ltd).

Characterization

The size and shape of synthesized nanoparticles and the morphologies of composite materials were observed using a scanning electron microscope (SEM, JSM-6700, JEOL) and field emission transmission electron microscope (FE-TEM, Tecnai G^2 20 F30 S-Twin, 300 kV). The crystal structures were analyzed using an X-ray diffractometer (XRD, D/MAX-2200V, Rigaku), and the chemical structural analysis was performed using X-ray photoelectron spectroscopy (XPS, K-Alpha, Thermo Fisher Scientific). The thermal-decomposition behavior of the nanoparticles was monitored using a thermal gravimetric analysis (TGA, SDT2960, TA Instruments). Electrochemical impedance spectra (EIS) analyses were conducted using a potentiostat (1287A, Solartron) and a frequency analyzer (1260, Solartron) with a four-probe configuration. The coin cells underwent initial charge/discharge cycles at a current density of 100 mA/g, and subsequently were allowed to equilibrate in open-circuit condition for 24 h to ensure homogeneous distribution of mobile species throughout each cell. After the equilibration, all EIS spectra were obtained with frequency range from 300 kHz to 0.01 Hz and AC amplitude of 10 mV.

Results and Discussion

The graphene oxides were prepared by a slightly modified Hummers method, and the resulting GO sheets were well-dispersed in an aqueous medium, showing a negative surface charge with a zeta potential ranging from -20 to -58 mV in overall pH range. Both CoO and Ag nanoparticles (NPs) were synthesized in amine-terminated organic solvents incorporating oleic acid as a capping molecule. The obtained olate-capped inorganic nanoparticles were readily dispersed in non-coordinating solvents. Both nanoparticles were individually separated without the formation of significant aggregates, showing a spherical morphology in shape (Figure S1). The diameter of Ag nanoparticles was measured to be 15 nm, and the CoO nanoparticles, with a diameter of 90 nm, consisted of 5-10 nm sized primary particles. The wet chemical synthesis of inorganic nanoparticles in non-coordinating solvents allows for the facile control of chemical synthetic paths, whereas the synthesis in aqueous media is indispensably associated with formation of hydroxide-involved intermediate phases. However, the water-soluble GO sheet was not compatible with organic solvents, while both inorganic nanoparticles were stabilized due to steric hindrance by freely elongated, surface-hydrocarbon chains. In our scheme for preparing the homogenous nanocomposites, the simple addition of co-solvent endowed the intermediate miscible phase of materials with distinctively different surface polarities. Without the incorporation of N-methyl-2-pyrrolidone (NMP), the aqueous GO solution and non-coordinating solvent-based Ag and CoO suspensions, were completely immiscible (Figure S2). However, by the addition of a proper amount of NMP, followed by a simple sonication-based agitation procedure, GO sheets were readily dispersed in Ag NP-dicholorobenzene (DCB) solution, forming a homogenous liquid phase (Figure 1a). Subsequently, the

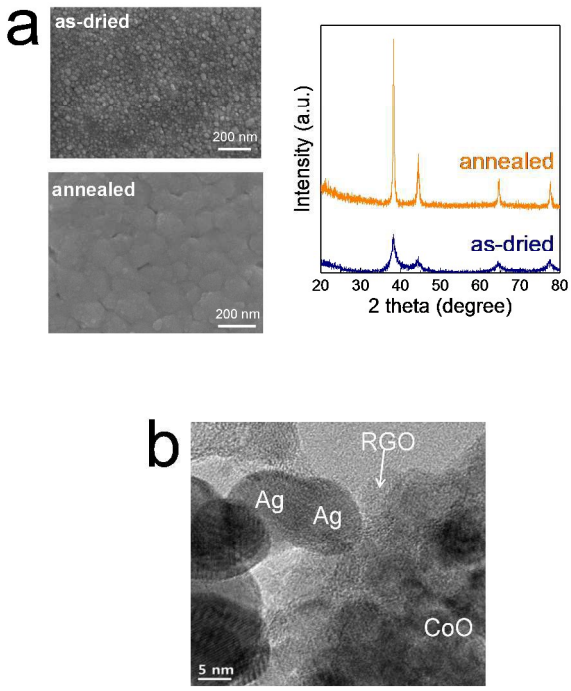

Figure 2. (a) SEM images and X-ray diffraction results for as-dried and thermally-annealed Ag nanoparticle films. Thermal annealing was carried out at 300 °C. (b) HRTEM image showing the local part of 3D-NCs, composed of Ag nanoparticles, CoO nanoparticles, and reduced graphene oxides.

addition of CoO NP-DCB solution together with simple agitation, facilitated the formation of aggregate-free, well-dispersed mixture solutions. Then, all the constituent materials were transformed into a uniformly condensed phase by centrifuging without supernatant.

The resulting precipitates were dried at 80 °C under vacuum, and annealed at 300 °C under Ar gas. It was clearly observed that the completely separated, individual GO sheets encapsulate the incorporated inorganic nanoparticles (Figure 1b). Note that the approach suggested in this paper is an easily accessible, one-pot chemical method for creating three-dimensional anodic electrodes without involvement of subsequent deposition processes, unlike previous methods such as formation of layer-by-layer structured films using a multiple vacuum filtration technique[20] and CNT growth on catalyst-anchored graphenes[21]. In general, after a drying process for extracting solvents from GO sheets individually separated in liquid phase, the GO sheets become stacked, losing their sheet-like surface property; to resolve this problem, a freeze-drying method or a specific solvent treatment should be involved.[22] However, with our composites, uniformly spaced inorganic nanoparticles enabled effective preservation of the inter-planar spacing between neighboring GO sheets after an easy, conventional drying process. This stacked nanostructure also makes it possible to wrap spatially the inner inorganic nanoparticles owing to the characteristic flexibility of individual GO sheets. From the HRTEM image (Figure 1c), it was also observed that CoO nanoparticles were uniformly loaded on the surface of GO sheets at a relatively high density, and that Ag nanoparticles were located between neighboring CoO nanoparticles, or at interfaces of CoO nanoparticles and GO sheets.

The Ag nanoparticles embedded in our nanocomposite have a role in forming completely stacked 3D structures. Each constituent in the as-dried CoO/GO/Ag composite is in physical contact with the others, but there is a lack of efficient charge transport pathways at inter-particular CoO junctions and at CoO/GO hetero-junctions. The Ag nanoparticles synthesized in this study undergo complete morphological transformation by thermal diffusion at 300 °C. The melting point (T_m) of Ag bulk phase is 921 °C. Heat treatment at temperatures approaching 0.8 x T_m is required to initiate atomic diffusion beyond the particle surfaces; but, as the size decreases below a few tens of nanometers, the onset temperature for morphological deformation diminishes drastically, depending on the diameter of metal nanoparticle.[23-25] As shown in Figure 2a, the as-dried particle assemblies, prepared by drop-casting a Ag-nanoparticle suspension onto a glass substrate, were evidently transformed into a fully connected film-like structure with extremely large grains, by atomic outward diffusion after annealing at 300 °C. Thermal decomposition of the capping molecules on the surface of Ag nanoparticles proceeded simultaneously during thermal annealing (Figure S3). Both phase-purity and drastic grain growth were also confirmed using XRD spectra. In them, the secondary phases were not detectable and the 'full width at half maximum' (FWMH) value decreased after annealing. Owing to its distinctive morphological properties after annealing at 300 °C, the electrical conductivity was measured to be 1.9×10^5 S/cm, whereas the as-dried film was electrically resistive. Nano-welding by thermally activated, diffused, metallic Ag phase was also confirmed in the CoO/GO/Ag nanocomposites (Figure 2b). During annealing at elevated temperatures under an inert gas, GO formed reduced-GO (RGO), as observed in XPS spectra for as-dried and for annealed GO powders (Figure S4 and Table S1). As for CoO nanoparticles, after annealing at 300 °C, the capping molecules were almost completely thermally decomposed (Figure S5), and the crystalline structure and morphological property did not vary (Figure S6). These results indicate that the well-formed, multilayered CoO/GO/Ag nanocomposite is converted into an electrically interconnected, three-dimensional CoO/RGO/Ag composite material by a thermally diffusible Ag nano-phase after simple, one-step annealing at 300 °C. As seen in X-ray diffraction result for annealed CoO/RGO/Ag nanocomposite (Figure S7), the crystalline structure for CoO and Ag nanoparticles were well preserved and the formation of partially reduced graphene oxide was observed with the 2-theta value of 21°.

The 3D intra-stacked CoO/RGO/Ag nanocomposite was tested for use as anodes in Li-ion batteries. The electrochemical measurements were carried out based on a half-cell configuration. The 3D intra-stacked CoO/RGO/Ag nanocomposite is referred to as 3D-NC. The proportion of CoO in 3D-NCs was maintained at 80 wt%, and above that, gradual degradation of electrochemical stability during repeated cycling tests occurred. At less than 80 wt%, the composition-dependent capacity decrement evolved due to the lack of electrochemically active sites (Figure S8 and S9). As control samples, the CoO and Ag nanoparticle-based anodes were tested, results from which confirmed that the CoO anode suffered from the significant fading behavior and that the Ag anode was almost electrochemically inactive (Figure S10). In our 3D-NCs, the control of composition is of paramount importance for attaining high-performance anodes. A proper balance leads to synergetic impact, as the CoO, Ag, and carbon phases play independent roles in determining the electrochemical performance of composite electrodes.

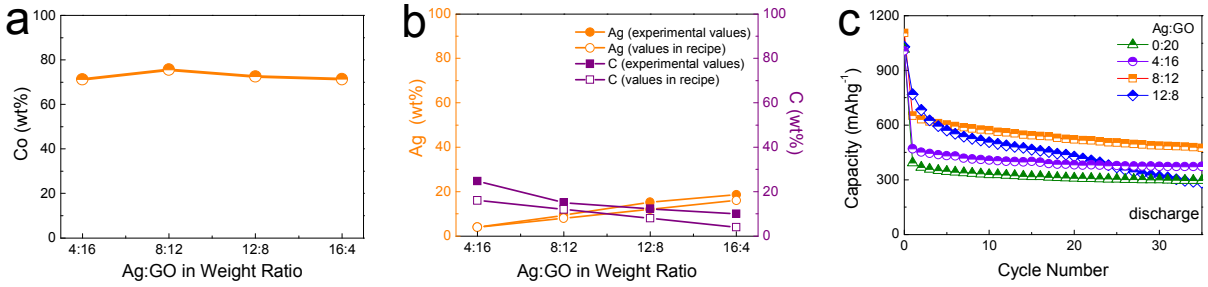

Figure 3. Variation in proportions of (a) CoO and (b) Ag and carbon in 3D-NCs prepared from batches with different weight ratios of Ag to GO. (c) Cycling performance for electrodes employing 3D-NCs with different weight ratios of Ag to GO. The current density was 100 mA/g. In the batches used for mixing Ag nanoparticles, CoO nanoparticles, and graphene oxides, a proportion of 80 wt% was maintained for CoO, and the weight ratios of Ag/GO were varied from 0/20 to 12/8.

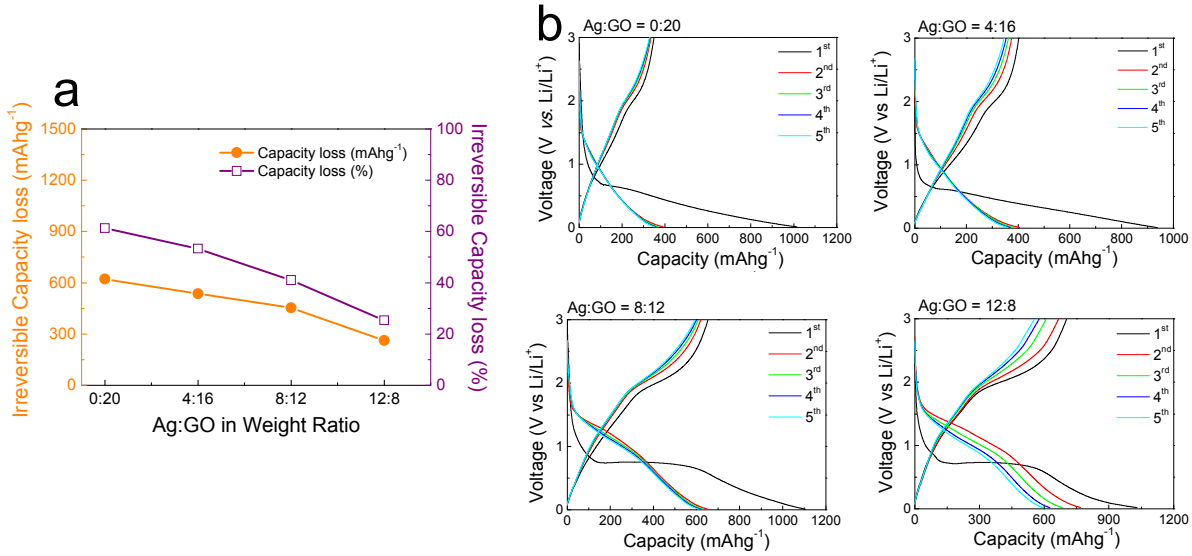

Figure 4. (a) Variation of irreversible capacity loss during a first cycle and (b) voltage profiles for electrodes employing 3D-NCs with different weight ratios of Ag to GO. The current density was 100 mA/g. In the batches used for mixing Ag nanoparticles, CoO nanoparticles, and graphene oxides, a proportion of 80 wt% was maintained for CoO, and the weight ratios of Ag/GO were varied from 0/20 to 12/8.

Interestingly, in our scheme, even though all hybridizing procedures were carried out in wet-solution batches in conjunction with a simple sonication-based mixing process, accurate control of composition was achievable to some extent. The proportion of CoO was almost unchanged with a value of 71–75 wt%, regardless of variation from 4/16 to 16/4 in the weight ratio of Ag to GO (Figure 3a). Moreover, the ratio of Ag to carbon was almost linearly adjustable depending on the weight ratio of Ag to GO (Figure 3b). The semi-accurate adjustment of composition in 3D-NCs was also confirmed by the fact that the electrochemical properties of CoO/Ag/GO anodes were varied, as expected from the role of each phase (Figure 3c). As the ratio of Ag to GO was varied from 0/20 to 12/8, the capacity in each first discharge state was almost identical (1006–1105 mAh/g). The proportion of CoO was maintained above 70 wt% in the 3D-NCs; the theoretical capacity of CoO is much higher than that of RGO, and the experimental capacity of the Ag nanoparticles synthesized in this study was below 150 mAh/g. Moreover, at the Ag/GO ratio of 12/8, the cycling fading was evolved, unlike other compositional anodes with enough amount of carbon compartment, indicative of the effective role of carbon phase in suppressing the morphological degradation, as described in previous studies.[3-7]

Notably, the capacity after repeated charge/discharge cycling tests was improved from ~300 to ~550 mAh/g when the ratio of Ag to GO was increased from 0/20 to 8/12, without significant cycle-fading behavior. This indicates that the Ag phase has a distinct role in 3D-NC electrodes. As shown in Figure 4, the irreversible capacity loss at first cycling was significantly improved as a function of the amount of Ag phase. As the ratio of Ag to GO was varied from 0/20 to 12/8, the irreversible capacity loss appeared to diminish from 622 to 261 mAh/g (a factor of 2.4), and the fraction of irreversible capacity loss with regard to the initial capacity, decreased from 61.3 to 25.3%. It has been recognized that for transition metal oxide-based anodic electrodes, the huge irreversible capacity is a

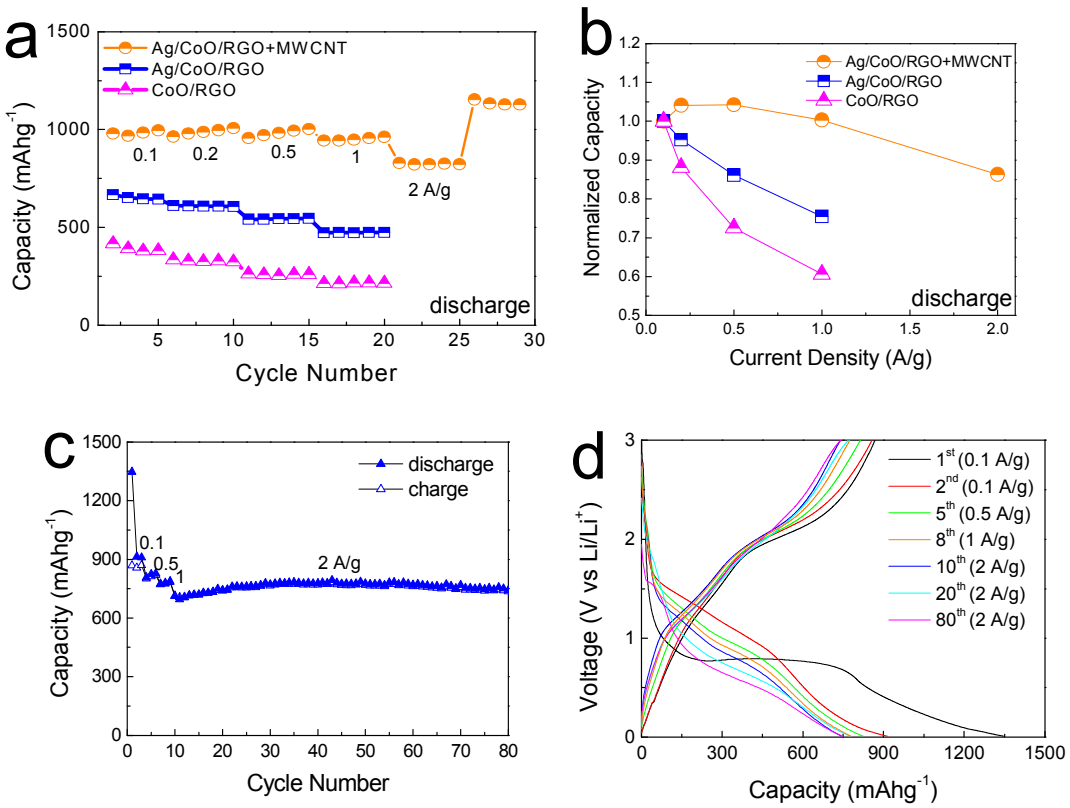

Figure 5. (a) Rate performance and (b) normalized capacity variation for electrodes employing Ag phase-free composite (CoO/RGO), 3D-NC, MWCNT incorporated 3D-NC. The ratios for Ag phase-free composite and 3D-NC were 80 (CoO): 20 (Ag) wt% and 80 (CoO): 8 (Ag): 12 (GO) wt%, respectively. (c) Cycling performance and (d) voltage profiles for MWCNT-incorporated 3D-NC composite electrodes at a current density of 2000 mA/g. Before reaching 2000 mA/g, the current density was increased incrementally during the first nine cycles.

heretofore-unresolved critical drawback in acquiring high capacity. Even so, no successful strategy for addressing this issue has been suggested. The proportion of Ag providing the best performance of 3D-NC was 8 wt%. Taking into consideration the density of CoO (6.44 g/cm^3), Ag (10.5 g/cm^3), and GO (2.62 g/cm^3 for carbon), the real volumetric proportion of the Ag phase in 3D-NC would be much less. This is indicative of the effective influence of the Ag phase in our 3D-NCs, in resolving the irreversible capacity issue. It is believed this result was obtained due to intact hetero-junctions formed by thermally driven nano-welding, along with the uniform spatial distribution of all constituent phases. Further study is underway to exploit Ag shell-structured metallic nanoparticles for addressing the economic issue of the Ag phase.

To clarify the roles of both electrically conductive pathways and nano-Ag phase in 3D nanocomposites, we also evaluated the rate capability of electrodes employing Ag phase-free nanocomposite (80 CoO: 20 RGO w/w), 3D-NC (80 CoO: 8 Ag: 12 RGO w/w), and multiwall carbon nanotube (MWCNT)-incorporated 3D-NC (80 CoO: 8 Ag: 12 RGO w/w). The MWCNTs were added when formulating the paste, as an additional conducting moiety along with carbon black, in order to provide electrical inter-pathways between neighboring 3D-NCs. As shown in Figure 5a, as the electrical inter- and intra-pathways developed, the rate capability improved significantly. The enhanced capacity of 3D-NC electrodes over Ag phase-free nanocomposite electrodes resulted from the aforementioned role of the Ag phase in suppressing the irreversible capacity. It is presumed that the increased capacity of MWCNT-incorporated 3D-NC electrodes (compared with bare 3D-NC electrodes), is attributable to increased generation of 3D-NCs in electrical contact with a current collector. This would result in a significant decrease in the number of electrically isolated 3D-NCs. Thus, the capacity (983 mAh/g at a current density of 100 mA/g) obtained with the MWCNT-incorporated 3D-NC electrodes, is believed to be close to a true value for our 3D-NC based electrodes. When a smaller amount of MWCNT was incorporated (1 wt% in a paste), the capacity was 770 mAh/g (Figure S11). The improvement in the rate capability was clearly observed in Figure 5b. The normalized capacity variation at current densities from 100 to 1000 mA/g was 0.4 and 0.25 for Ag phase-free nanocomposite and 3D-NC electrodes, respectively, and this is indicative

determining influence of electrical intra-pathways in the composite materials. For MWCNT-incorporated 3D-NC electrodes, at current densities from 100 to 2000 mA/g, the normalized capacity variation was merely 0.14. This is additional critical evidence of the importance of establishing electrical inter-pathways between hierarchically structured composites, as well as the intra-pathways inside them. As a control, a sample of Ni/CoO/RGO composite was synthesized by replacing Ag nanoparticles with Ni nanoparticles during preparation of 3D-NCs. The cycling performance, rate performance, and voltage profiles for electrodes employing MWCNT-incorporated Ni/CoO/RGO composites, are shown in Figure S12. The material ratio in a mixing batch was 80 (CoO nanoparticle): 8 (Ni nanoparticle): 12 (GO) wt%. The thermal annealing needed to complete the preparation of the composite materials, was carried out at 400 ^{o}C. The 30-nm-sized Ni nanoparticles underwent structural welding at a high temperature, by virtue of a relatively larger particle size, and due to the presence of a surface oxide layer (Figure S13). The electrochemical performances similar to those of Ag phase-involved 3D-NC composite electrode were obtained, except for the irreversible capacity loss of 578 mAh/g during a first discharging/charging cycle. This indicates that both the high initial capacity and the excellent rate capability are obtainable via formation of uniform carbon-based composites including electrochemically active transition-metal oxides and electrically conductive pathways, and the improvement in the irreversible capacity would evolve due to the characteristic catalytic effect of the Ag phase.

Figure 5c shows the cycle performance and voltage profiles for MWCNT-incorporated 3D-NC electrodes at a current density of 2000 mA/g. In the initial cycles, stepwise increments in current density were applied and current density of 2000 mA/g was applied over 10 cycles. It was clearly observed that high capacity (~770 mA/g) was stably maintained even when current density was high. In this study, capacity was calculated based on the total weight of active materials, without excluding the weight of carbons in composite materials. Note that for metal oxide-based anodes, to date, such high capacity (approaching 800 mAh/g at a current density of 2000 mA/g) has been achievable only with binder-free 3-D electrodes using pre-structured conductive supports; electrodes employing $ZnCo_2O_4$ nanowires hydrothermally-grown on perfectly structured carbon cloth reached a capacity of 710 mA/g at a current density of 1800 mA/g,[26] and a capacity of ~500 mA/g at a current density of 2500 mA/g, was reported for electrodes composed of vacuum-deposited SnO_2 on conductive nickel nanofoams.[27]

To gain further insight into the origins of different aspects of electrochemical performance in nanocomposite electrodes, electrochemical impedance spectra (EIS) analyses were carried out for cells employing Ag phase-free CoO/RGO nanocomposite, 3D-NC, and MWCNT-incorporated 3D-NC (Figure 6a). The measurements were performed after an initial charge/discharge cycle in order to exclude the irreversible reaction stage, at which both solid electrolyte interphase (SEI) formation and irreversible conversion reactions occur. The impedance response of LIBs can be regarded as the sum of following processes: (i) conduction of Li ions and electrons (R_{ohmic}), (ii) Li-ion migration through the SEI layer (R_{SEI}, CPE_{SEI}), (iii) charge transfer-involved electrochemical reaction of active materials (R_{ct}, CPE_{ct}), and (iv) Li-ion diffusion into the lattice of active materials (W). They can be expressed as an equivalent circuit, as shown in Figure 6b. All three cells

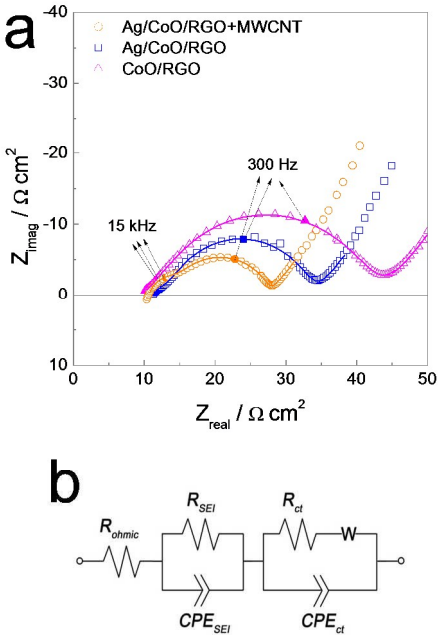

Figure 6. (a) EIS spectra of cells based on the Ag phase-free CoO/RGO nanocomposite, 3D-NC and MWCNT-incorporated 3D-NC. (b) Equivalent circuit model employed to deconvolute the EIS spectra. The numbers in the Nyquist plot represents the characteristic frequencies for polarizations due to the SEI layer and a charge transfer reaction. The letters *R, CPE,* and W stand for resistor, constant phase element, and Warburg diffusion element, respectively. The subscripts of *SEI* and *ct* denote the solid electrolyte interphase and the charge transfer reaction, respectively.

exhibited similar ohmic resistance (~10 Ωcm^2) because the resistance in Li-ion transport is much higher than that of electron-charge transport. The morphological structures that determine the spatial distribution of liquid electrolyte, did not vary significantly between the three composite materials. It was clearly observed that the polarization resistance was highly dependent on the kind of composite material considered. Employing the equivalent circuit, the polarization resistance could be explained in terms of SEI-layer formation and electrochemical reaction rate. It was revealed that the R_{SEI} is influenced by the presence of welded Ag phase. The value of R_{SEI} for a Ag phase-free composite (CoO/RGO)-based cell was 13.9 Ωcm^2, while the introduction of the Ag phase in the 3D-NC-based cell, decreased drastically the value of R_{SEI} (to 3.9 Ωcm^2). For MWCNT-incorporated 3D-NC, the value of R_{SEI} was approximated by the value of 3.6 Ωcm^2. This implies that the Ag phase plays critical roles in suppressing the evolution of the SEI layer, effectively diminishing the irreversible capacity loss as well as in establishing internal electrical pathways, as observed in the aforementioned electrochemical performance. Interestingly, R_{ct} was measured to be 21.2, 17.3, and 13.2 Ωcm^2 for cells based on Ag phase-free CoO/RGO nanocomposite, 3D-NC, and MWCNT-incorporated 3D-NC, respectively. Such gradual decrement in R_{ct} is associated with increase in volumetric density of an active two-phase boundary, where the charge transfers for electrochemical reactions occur. This provides reasonable evidence to support the fact that a huge increment in capacity evolves in cells employing MWCNT-incorporated 3D-NC. When RGO was replaced with Ag phase,

the improvement in capacity was compensated to some extent due to the electrochemically inactive nature of the Ag phase tested in this study, along with the beneficial effect in reducing the resistance of charge transfer.

Conclusions

We have reported the methodology for deriving high-performance anodic materials by a one-pot wet-chemical method based on an easily accessible, sono-chemical process. All the constituent materials (i.e., CoO nanoparticles, reduced graphene oxides, and Ag nanoparticles) were incorporated homogeneously, and each played a distinct role in the three-dimensionally intra-stacked nanocomposite. It was revealed that the unique partial-melting nature of 15 nm-sized Ag nanoparticles allows for the formation intra-welded homogenous composites, enabling for the distinct suppression of irreversible capacity loss from 622 to 261 mAh/g, along with the contribution of electrochemically active CoO phase for high capacities and of individually separated carbon sheets for high cycling stability. The high performance was demonstrated, with capacities of 983 and 770 mAh/g, at current densities of 100 and 2000 mA/g, respectively, and the interpretation for comparative studies of compositional composites, have clarified the paramount importance of architectural design in hierarchically structured nanocomposite materials.

Acknowledgements

This research has been supported by the Korea Research Institute of Chemical Technology (KRICT), and partially supported by a grant from the National Research Foundation of Korea funded by the Korean government (MISP) (NRF-2010-0028971).

Notes and references

[a] Division of Advanced Materials, Korea Research Institute of Chemical Technology (KRICT), Daejeon 305-600, Republic of Korea
E-mail: shochoi@krict.re.kr (S. Choi); sunsukl@krict.re.kr (S. S. Lee); sjeong@krict.re.kr (S. Jeong)
[b] Department of Materials Science and Engineering, Yonsei University, 50 Yonsei-ro Seodaemun-gu, Seoul, 120-749, Republic of Korea

Electronic Supplementary Information (ESI) available: Details for C 1s core level spectra for 3D-NCs, images for Ag and CoO nanoparticles, photographs showing the miscibility/immiscibility for prepared suspensions, TGA results for Ag and CoO nanoparticles, XPS C 1s spectra for 3D-NCs, cycling performances and voltage profiles for anodes employing 3D-NCs with different compositions, cycling performances and voltage profiles for anodes with a paste composition of 1 wt% MWCNT, and cycling performances and voltage profiles for anodes employing Ni nanocomposites. See DOI: 10.1039/b000000x/

1 V. Etacheri, R. Marom, R. Elazari, G. Salitra and D. Aurbach, *Energy Environ. Sci.* 2011, **4**, 3243-3262.
2 M. V. Reddy, G. V. Subba and B. V. R. Chowdari, *Chem. Rev.* 2013, **113**, 5364-5457.
3 Z. S. Wu, W. Ren, L. Wen, L. Gao, J. Zhao, Z. Chen, G. Zhou, F. Li and H. M. Cheng, *ACS Nano*, 2010, **4**, 3187-3194.
4 J. Liang, Y. Zhao, L. Guo and L. Li, *ACS Appl. Mater. Interfaces*, 2012, **4**, 5742-5748.
5 J. Zhu, Y. K. Sharma, Z. Zeng, X. Zhang, M. Srinivasan, S. Mhaisalkar, H. Zhang, H. H. Hng and Q. Yan, *J. Phys. Chem. C*, 2011, **115**, 8400-8406.
6 S. Q. Chen and Y. Wang, *J. Mater. Chem.*, 2010, **20**, 9735-9739.
7 C. T. Hsieh, J. S. Lin, Y. F. Chen and H. Teng, *J. Phys. Chem. C*, 2012, **116**, 15251-15258.
8 J. Ming, J. B. Park and Y. K. Sun, *ACS Appl. Mater. Interfaces*, 2013, **5**, 2133-2136.
9 W. Luo, X. Hu, Y. Sun and Y. Huang, *ACS Appl. Mater. Interfaces*, 2013, **5**, 1997-2003.
10 G. Ji, B. Ding, Z. Sha, J. Wu, Y. Ma and J. Y. Lee, *Nanoscale*, 2013, **5**, 5965-5972.
11 H. Lai, J. Li, Z. Chen and Z. Huang, *ACS Appl. Mater. Interfaces*, 2012, **4**, 2325-2328.
12 L. Pan, H. Zhao, W. Shen, X. Dong and J. Xu, *J. Mater. Chem. A*, 2013, **1**, 7159-7166
13 S. Yang, X. Feng, S. Ivanovici and K. Mullen, *Angew. Chem. Int. Ed.*, 2010, **49**, 8408-8411.
14 X. Zhu, Y. Zhu, S. Murali, M. D. Stoller and R. S. Ruoff, *ACS Nano*, 2011, **5**, 3333-3338.
15 W. H. Ryu, J. Shin, J. W. Jung and I. D. Kim, *J. Mater. Chem. A*, 2013, **1**, 3239-3243.
16 L. Zhang, G. Zhang, H. B. Wu, L. Yu and X. W. Lou, *Adv. Mater.*, 2013, **25**, 2589-2593.
17 W. Wei, S. Yang, H. Zhou, I. Lieberwirth, X. Feng and K. Mullen, *Adv. Mater.*, 2013, **25**, 2909-2914.
18 C. Chae, J. H. Kim, J. M. Kim, Y. K. Sun and J. K. Lee, *J. Mater. Chem.*, 2012, **22**, 17870-17877.
19 L. Zeng, C. Zheng, C. Deng, X. Ding and M. Wei, *ACS Appl. Mater. Interfaces*, 2013, **5**, 2182-2187.
20 A. Yu, H. W. Park, A. Davies, D. C. Higgins, Z. Chen and X. Xiao, *J. Phys. Chem. Lett.*, 2011, **2**, 1855-1860.
21 S. H. Lee, V. Sridhar, J. H. Jung, K. Karthikeyan, Y. S. Lee, R. Mukherjee, N. Koratkar and I. K. Oh, *ACS Nano*, 2013, **7**, 4242-4251.
22 Y. Yoon, K. Lee, S. Baik, H. Yoo, M. Min, Y. Park, S. M. Lee and H. Lee, *Adv. Mater.*, 2013, **25**, 4437-4444.
23 Y. Jo, S. Oh, S. S. Lee, Y. H. Seo, B. H. Ryu, Y. Choi and S. Jeong, *J. Mater. Chem. C*, 2014, 2, 9746-9753.
24 S. Jeong, S. H. Lee, Y. Jo, S. S. Lee, Y. H. Seo, B. W. Ahn, G. Kim, J. U. Jang, Y. Choi and B. H. Ryu, *J. Mater. Chem. C*, 2013, **1**, 2704-2710.
25 S. Jeong, H. C. Song, W. W. Lee, H. J. Suk, S. S. Lee, T. Ahn, J. W. Ka, Y. Choi, M. H. Yi and B. H. Ryu, *J. Mater. Chem.*, 2011, **21**, 10619-10622.
26 B. Liu, J. Zhang, X. Wang, G. Chen, D. Chen, C. Zhou and G. Shen, *Nano Let.*, 2012, **12**, 3005-3011.
27 J. M. Haag, G. Pattanaik and M. F. Durstock, *Adv. Mater.*, 2013, **25**, 3238-3243.

